Structural Solution of Mesocaged Material AMS-8

Alfonso E. Garcia-Bennett,* Keiichi Miyasaka, and Osamu Terasaki

Structural Chemistry, Arrhenius Laboratory, Stockholm University, S-10691 Stockholm, Sweden

Shunai Che

Department of Chemistry, School of Chemistry and Chemical Technology, Shanghai Jiao Tong University, 800 Dongchuan Road, Shanghai, 200240, P. R. China

Received April 14, 2004. Revised Manuscript Received June 16, 2004

A novel mesoporous material prepared using the recently reported co-assembly of anionic surfactants with organosilane groups has been studied in depth using high-resolution transmission electron microscopy (HRTEM) and electron crystallography. A three-dimensional (3D) structural solution of AMS-8 was obtained by Fourier analysis of HRTEM images, revealing a complex cubic mesocaged solid (space group $Fd\bar{3}m$) composed of bimodal cages 3D-connected by cage windows. HRTEM images also indicate the presence of structural defects associated with the cubic close packing of spheres, while analysis by nitrogen adsorption−desorption isotherms reveals that accessibility to smaller cages may be restricted in this material. The opened and closed models of this structure derived from a combination of electron crystallography and nitrogen adsorption data are discussed with respect to the arrangement of cages and cage connectivities. Considerations of the nature of the micellar system playing part in this novel templating mechanism are discussed.

Introduction

Mesoporous materials have evolved considerably since the first reported preparation more than a decade ago.[1] Advancements from a synthetic, characterization, and applications perspective have given rise to a rapidly developing field centered on the co-assembly of surfactant molecules with silica and non-siliceous precursors. The use of polymer surfactants, for example, have allowed expansion of the pore size to larger sizes,[2] while applications in chemical sensing, photocatalysis, and optics are currently being investigated.[3] The use of silica mesoporous solids as hard templates for carbon replicas and polymer−carbon composites is also attracting a lot of interest as the resultant materials exhibit surface properties of the polymer as well as the electric conductivity of the carbon framework, which could provide new possibilities for advanced applications.[4]

A novel route for the synthesis of high-quality mesoporous silicates using anionic surfactants and organosilane groups as co-structure directing agents has been recently reported by Che et al.[5] The use of anionic surfactants to direct the self-assembly of cationic and anionic metal oxide (M+) species has been reported previously based on covalent bond formation, but these preparations have resulted only in lamellar and disordered structures.[6]

This new synthesis pathway relies on increased interaction between the condensing silica framework and the self-assembling anionic surfactant. This is achieved, under alkaline conditions, via the negatively charged carboxylic headgroup of the anionic surfactant and the ammonium site of the organoalkoxysilane co-structure directing agents (CSDA) *N*-trimethoxysilylpropyl-*N*,*N*,*N*-trimethylamonium chloride (TMAPS) and 3-aminopropyltrimethoxysilane (APS). This family of materials has been named AMS-n (Anionic surfactant templated Mesoporous Silicas). The mechanism has been generalized as $S^-N^+{\sim}I^-$, where S^- is the surfactant, N^+ represents the positively charged amine moiety in the aminosilane group, and I^- is the condensing silica framework.

Initial HRTEM and XRD studies show that a wider structural diversity is observed in mesoporous materials synthesized using anionic surfactant systems. It has been shown, for example, that 2D-/3D-hexagonal (AMS-3 and AMS-1, respectively), 3D-cubic (AMS-2, AMS-4, AMS-6, and AMS-8), lamellar (AMS-5), and disordered mesophases (AMS-7) can be easily prepared through variations in anionic surfactant, co-structure directing agent (CSDA), and synthetic conditions.[7] In addition, structural characteristics unprecedented in mesoporous solids have been observed by electron microscopy. Of particular interest are local structural modulations in the 3D-cubic mesostructure AMS-2, a caged structure

* To whom correspondence should be addressed. E-mail: alf@struc.su.se.

(1) Kresge, C. T.; Leonowicz, M. E.; Roth, W. J.; Vartulli, J. C.; Beck, J. S. *Nature* **1992**, *359*, 710.
(2) Zhao, D. Y.; Huo, Q.; Feng, J.; Kim, J.; Han, Y.; Stucky, G. D. *Chem. Mater.* **1999**, *11*, 2668.
(3) Schüth, F. *Chem. Mater.* **2001**, *13*, 3184.
(4) Choi, M.; Ryoo, R. *Nature Mater.* **2003**, *2*, 473.
(5) Che, S.; Garcia-Bennett, A. E.; Yokoi, T.; Sakamoto, K.; Kunieda, H.; Terasaki, O.; Tatsumi, T. *Nature Mater.* **2003**, *2*, 801.
(6) Wong, M. S.; Ying, J. Y. *Chem. Mater.* **1998**, *10*, 2067. Antonelli, D. M.; Ying, J. Y. *Angew. Chem., Int. Ed. Engl.* **1996**, *35*, 426.
(7) Garcia-Bennett, A. E.; Che, S.; Tatsumi, T.; Terasaki, O. *Chem. Mater.* **2004**, *16*, 813.

10.1021/cm049398e CCC: $27.50
Published on Web 08/26/2004

similar to SBA-1,[8] the intergrowth structure of AMS-4 showing both 3D-hexagonal and 3D-cubic stacking arrangements of cages, and the flat-shaped spherical morphology of AMS-6, having analogous structure with the much studied MCM-48 and FDU-5 bicontinuous cubic mesophases synthesized with cationic and polymeric surfactants, respectively.[9,10] Synthetic and structural investigations of these materials are being conducted to determine the effect of preparation conditions on structural characteristics, pore connectivity, growth mechanisms, and morphology. Our findings will be reported shortly.

The present study concerns the 3D-cubic structure known as AMS-8. Our preliminary investigations by HRTEM imaging and electron diffraction suggest this material to be a completely new mesostructure, with space group symmetry $Fd\bar{3}m$ (or *Fd3* but assumed to be the former, which is of higher symmetry).

Surfactant liquid-crystal phases exhibiting $Fd\bar{3}m$ symmetry have been reported previously, but these are thought to occur only in inverse micellar cubic phases.[11] These phases are composed of two differently sized types of micelle and they are more prominent in binary lipid systems. Each type of lipid forms one particular size of inverse micelle, where one is very weakly hydrophilic (for example, a fatty acid). This is thought to allow the partial separation of the two lipid components into two micelle systems, with the less hydrophilic species located preferentially in the smaller more negatively curved inverse micelles. The unit cell consists of 8 larger and 16 smaller quasi-spherical inverse micelles.[12] In the context of mesoporous materials, however, it is hard to envisage an inverse micelle system templating a silicate structure under the conditions of synthesis employed here (aqueous conditions, low surfactant concentration, and the presence of co-structure directing agent). Our hypothesis is that a two-micelle system is indeed formed but normal micelles are present.

A silicate mesoporous structure with $Fd\bar{3}m$ symmetry has been reported previously in the literature, although this work does not cite sufficient information to describe the pore arrangement or connectivity in the cubic structure.[13]

To fully elucidate the internal pore structure and determine the connectivity and shape of pores/cages in AMS-8, we have carried out structural investigations by electron microscopy and electron crystallography. In 2000, Sakamoto et al.[14] conducted pioneering work into the structural solution of mesoporous materials by

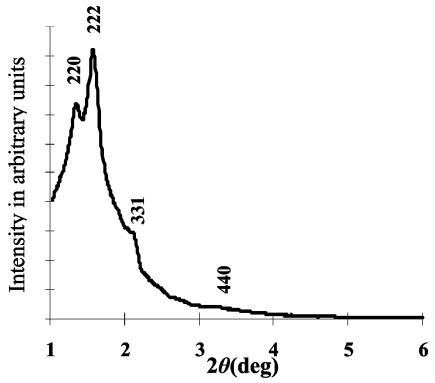

Figure 1. X-ray diffraction pattern of calcined AMS-8 cubic mesocaged structure with unit cell parameter $a = 183.4$ Å.

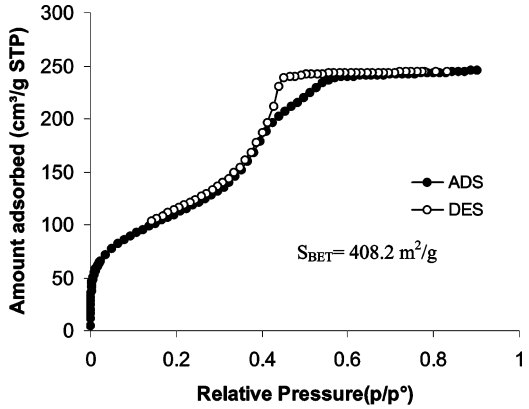

Figure 2. Nitrogen adsorption−desorption isotherm of calcined AMS-8. The isotherm shows a relatively broad capillary condensation step accompanied by a marked hysteresis effect in desorption branch of the isotherm.

electron crystallography, based on the 3D-Fourier transform (FT) reconstruction of electron crystallography data. This procedure has been described at length elsewhere.[15,16] The 3D structures of silicate mesoporous solids MCM-48 ($Ia\bar{3}d$), SBA-1 ($Pm\bar{3}n$), SBA-6 ($Pm\bar{3}n$), SBA-12 ($Fm\bar{3}m$), SBA-16 ($Im\bar{3}m$), and the carbon-replica CMK-type materials have been investigated in this way.[14−16]

A large amount of effort has been recently devoted to the characterization of mesoporous materials using nitrogen adsorption data and to extend the applicability of this technique to mesocaged materials.[17] The BJH model of pore size analysis has been proven to underestimate the pore size mesoporous materials by as much as 100% when caged structures are considered, and to be inapplicable to determine pore size distributions below 30 Å, because of its dependence on the modified Kelvin equation. Recently, Ravikovitch et al. developed a method based on nonlocal density functional theory (NLDFT) for the characterization of mesocaged struc-

(8) Huo, Q.; Margolese, D. I.; Ciesla, U.; Demuth, D. G.; Feng, P.; Gier, T. E.; Sieger, P.; Leon, R.; Petroff, P. M.; Schüth, F.; Stucky, G. D. *Nature* **1994**, *368*, 317.

(9) Kaneda, M.; Tsubakiyama, T.; Carlsson, A.; Sakamoto, Y.; Ohsuna, T.; Terasaki, O.; Joo, S. H.; Ryoo, R. *J. Phys. Chem. B* **2002**, *106*, 1256.

(10) Liu, X.; Tian, B.; Yu, C.; Gao, F.; Xie, S.; Tu, B.; Che, R.; Peng, L.; Zhao, D. Y. *Angew. Chem., Int. Ed.* **2002**, *41*, 3876.

(11) Luzzati, V.; Vargas, R.; Gulik, A.; Mariani, P.; Seddon, J. M.; Rivas, E. *Biochemistry* **1992**, *31*, 279. Delacroix, H.; Gulik-Krzywicki, T.; Seddon, J. M. *J. Mol. Biol.* **1996**, *258*, 88. Alexandridis, P.; Olsson, U.; Lindman, B. *Langmuir* **1998**, *14*, 2627.

(12) Seddon, J. M.; Templer, R. H. In Polymorphism of Lipid-Water Systems. *Handbook of Biological Physics, Volume 1*; Lipowsky, R., Sackmann, E., Eds.; Elsevier Science B. V.: New York, 1995.

(13) Shen, S.; Li, Y.; Zhang, Z.; Fan, J.; Tu, B.; Zhou, W.; Zhao, D. *Chem. Commun.* **2002**, (19), 2212.

(14) Sakamoto, Y.; Kaneda, M.; Terasaki, O.; Zhao, D.; Kim, J.-M.; Stucky, G. D.; Shin, H. J.; Ryoo, R. *Nature* **2000**, *408*, 449.

(15) Carlsson, A.; Kaneda, M.; Sakamoto, Y.; Terasaki, O.; Ryoo, R.; Joo, S. H. *J. Electron Microsc.* **1999**, *48*, 795.

(16) Sakamoto, Y.; Diaz, I.; Terasaki, O.; Zhao, D.; Perez-Pariente, J.; Kim, J. M.; Stucky, G. D. *J. Phys. Chem. B* **2002**, *106*, 3118. Kaneda, M.; Tsubakiyama, T.; Carlsson, A.; Sakamoto, Y.; Ohsuna, T.; Terasaki, O.; Joo, S. H.; Ryoo, R. *J. Phys. Chem. B* **2002**, *106*, 1256.

(17) Ravikovitch, P. I.; Haller, L. G.; Neimark, A. *Adv. Colloid Interface Sci.* **1998**, *76*, 203. Lukens, W.; Schmidt-Winkel, P.; Zhao, D.; Feng, J.; Stucky, G. D. *Langmuir* **1999**, *15*, 5403. Kruk, M.; Jaroniec, M. *Chem. Mater.* **2003**, *15*, 2942. Garcia-Bennett, A. E.; Williamson, S.; Wright, P. A.; Shannon, I. J. *J. Mater. Chem.* **2002**, *12*, 3533.

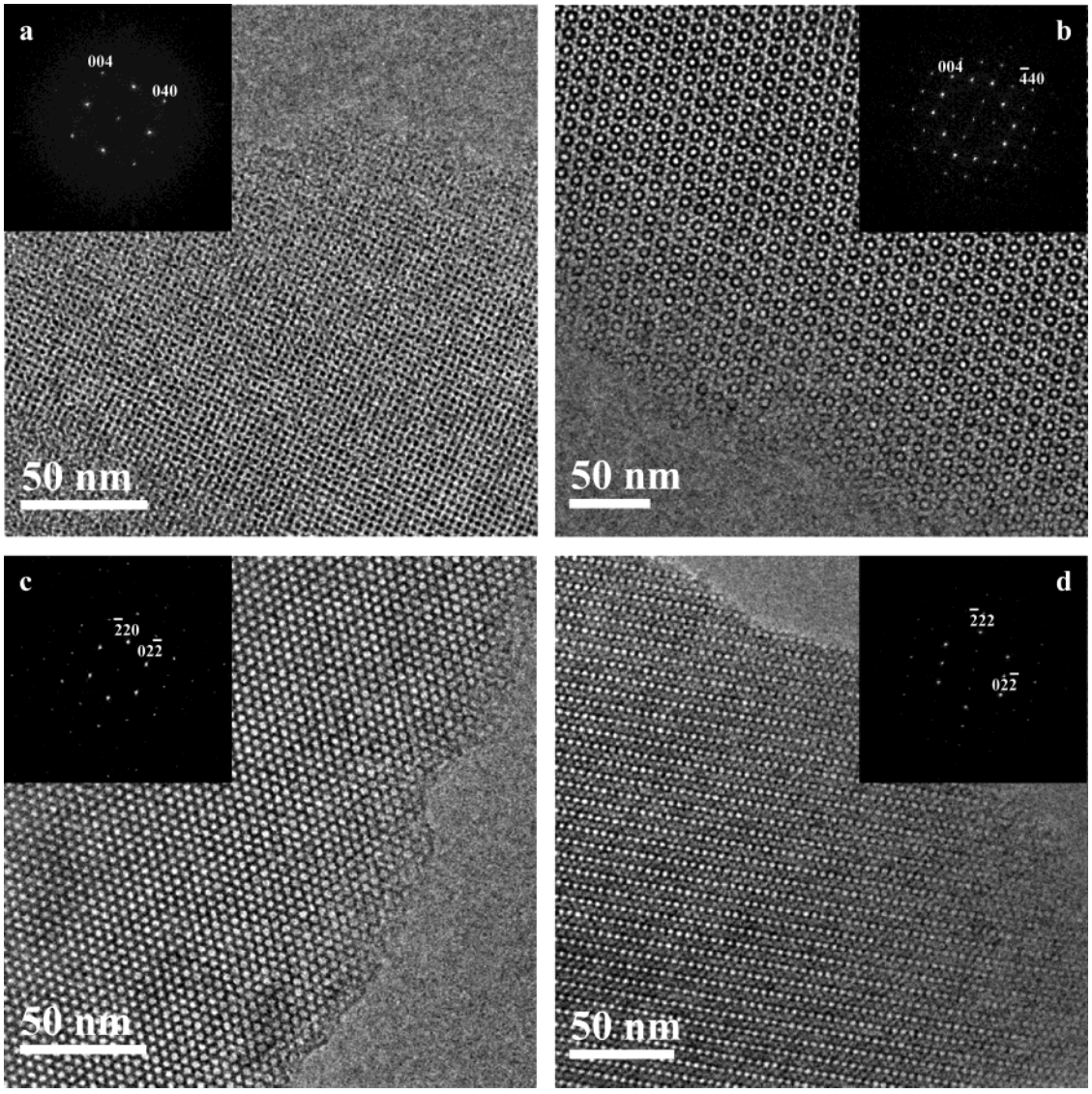

Figure 3. Typical HRTEM images and corresponding FT diffractograms of calcined AMS-8 recorded with (a) [100], (b) [110], (c) [111], and (d) [211] incidence. Diffractograms are indexed on the basis of a cubic unit cell, $a = 177.9$ Å. All images show large ordered regions indicative of a well-structured material.

Table 1. Structural and Porosity Data for Calcined AMS-8 as Derived from Several Characterization Methods, Where the "Connectivity" Refers to the Window Size between Cages

method	unit cell parameter (Å)	mesopore volume (cm^3/g)	large cage (L) (Å)	small cage (S) (Å)	connectivity L and L cages (Å)	connectivity L and S cages (Å)	connectivity S and S cages (Å)	surface area (m^2/g)
XRD	183.4							
N_2 adsorption								
NLDFT		0.361	55.0	37.0	13.6	<10.0	<10.0	584.2
HK		0.364	56.4	40.0	6.2	6.2	–	408.2[a]
TEM								
FT-reconstruction threshold 189	177.9	0.365	75.0	52.0	14.0	–	–	366.4
FT-reconstruction threshold 199	177.9	0.424	76.0	56.0	25.0	5.0	5.0	411.3

[a] BET surface area.

tures.[18,19] NLDFT pore size distribution curves give accurate information about the size of cages, the total meso-/micropore volumes and surface area, and in combination with the X-ray diffraction (XRD) measurements the pore wall thickness. In sufficiently small cavities (pore diameters $3 < D < 6$ nm) capillary condensation occurs reversibly, and the equilibrium condensation pressure is determined by the diameter of the cavity. Furthermore, it is suggested that if the window connecting cavities is smaller than a certain critical size (ca. 4 nm for N_2 at 77 K) or the equilibrium evaporation pressure from the pore window is lower than a certain critical relative pressure, the confined fluid will reach its limit of stability, and spontaneous desorption occurs. In other words the desorption condi-

(18) Tarazona, P. *Phys. Rev. A* **1985**, *31*, 2672.
(19) Ravikovitch, P. I.; Wei, D.; Chueh, W. T.; Haller, G. L.; Neimark, A. V. *J. Phys. Chem. B* **1997**, *101*, 3671. Ravikovitch, P. I.; Neimark, A. V. *Langmuir* **2002**, *18*, 1550. Ravikovitch, P. I.; Neimark, A. V. *Langmuir* **2000**, *16*, 2419.

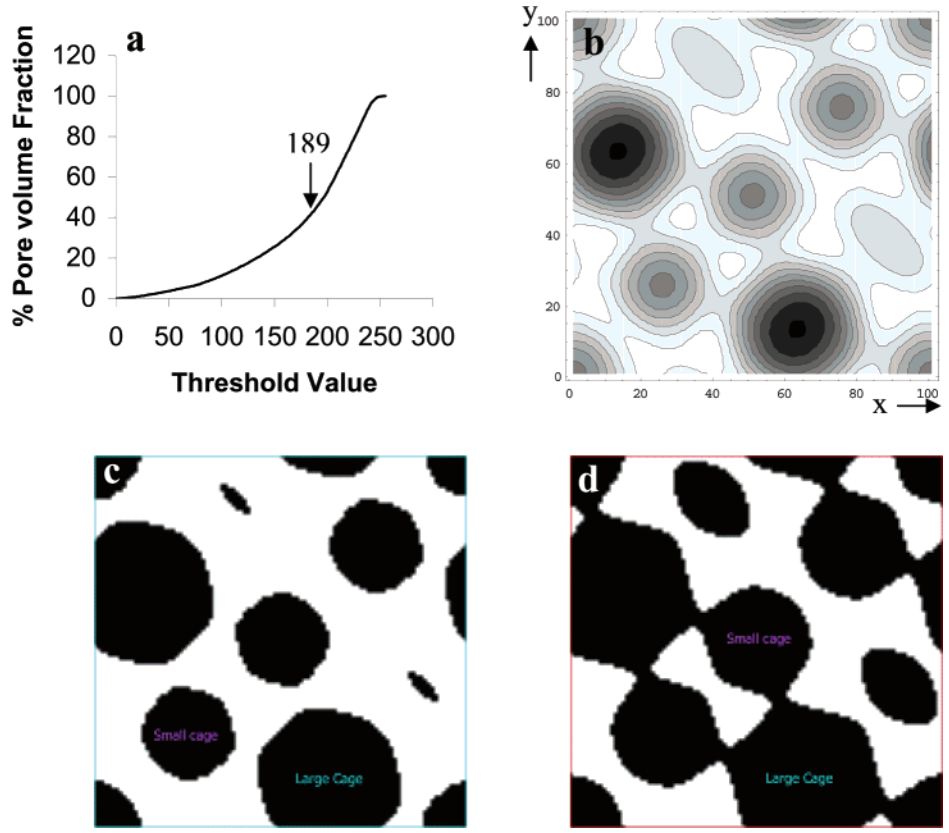

Figure 4. Plot of pore volume fraction versus potential density of the wall for mesocaged material AMS-8 (a), from which the 2D-sliced electrostatic potential density maps of the unit cell can be derived for the threshold range 150−256 (b) and the threshold values 189 (c) and 199 (d). The latter correspond to 44 and 50% pore volume fractions, respectively. The unit cells slices are taken with $z = 7$, where the unit cell has been divided into 100 slices (slice thickens = 1.834 Å). White contrast represents the silica wall and black contrast represents the pore space.

Table 2. Observed 3D-Crystal Structure Factors of AMS-8 after Correction of CTF

h	*k*	*l*	F_{hkl}/F_{110} (%) CTF	phase	*h*	*k*	*l*	F_{hkl}/F_{110} (%) CTF	phase
1	1	1	81.78	0	6	4	2	−0.53	π
2	2	0	−100.00	π	6	4	4	0.17	0
2	2	2	73.15	0	6	6	0	−0.39	π
3	1	1	77.28	0	6	6	2	−0.41	π
3	3	1	17.02	0	6	6	4	0.46	0
3	3	3	10.72	0	6	6	6	0.11	0
4	0	0	33.07	0	7	1	1	−0.85	π
4	2	2	−13.17	π	7	3	1	0.56	0
4	4	0	−10.26	π	7	3	3	0.46	0
4	4	2	−3.77	π	7	5	1	−0.13	π
4	4	4	−2.12	π	7	5	5	−0.35	π
5	1	1	9.83	0	7	7	1	−0.15	π
5	3	1	−1.84	π	7	7	3	−0.08	π
5	3	3	0.51	0	7	7	5	−0.12	π
5	5	1	0.96	0	8	0	0	0.07	0
5	5	3	0.09	0	8	2	2	−0.28	π
5	5	5	−0.16	π	8	4	0	0.06	0
6	2	2	−1.70	π					

tion can be related to the size of cage windows. Applying this method, Kleitz et al. recently reported the characterization of cages and cage openings in the cubic mesostructure FDU-1, estimating apertures of mesoporous cavities to be <5.0 nm by considering the spinodal evaporation observed in the desorption branch of the isotherm indicated by an hysteretic effect.[20]

Accurate structural and porous information is of great importance for the development of mesoporous materials in applications such as catalysis, for example, in petroleum refinement, acid catalyst, redox reaction catalyst, and pollution control. Mesoporous materials with ordered pore structures and defined pore connectivity can be utilized as ideal nanoreactors to confine the growth of nanomaterials and in gas separation. For these applications the window connecting cages may impart a degree of specificity (or hindrance), allowing tailoring of mesocaged materials to specific reactants and products. In addition, this information allows us to assess the potential of specific structure types in terms of surface area, pore size, connectivity, and the effect of structural defects on these parameters, allowing for control and design of more complex porous networks.

Experimental Section

The synthesis of mesoporous AMS-8 has been reported previously. In a typical synthesis 0.2 g of sodium *N*-lauroyl-L-glysine were dissolved in 20 mL of deionized water with stirring at 60 °C. To this solution 0.36 g of TMAPS co-structure directing agent were added with rapid agitation (300 rpm), followed by the addition of 1.5 g of tetraethyl orthosilicate (TEOS) to give a final TEOS:TMAPS:C_{12}Glysine:H_2O molar ratio in the gel of 1:0.1:0.1:155. The pH of the reaction gel was measured to be 10. The resultant silica gel solution was stirred for a period of 5−10 min to promote the hydrolysis of the co-structure directing agent and the silicate precursor. The reaction gel was then allowed to stand at 100 °C for 3 days with no stirring. After the reaction was complete, the AMS-8 precipitate was filtered, washed with 100 mL of H_2O, and dried overnight at room temperature. Removal of the surfactant was conducted by calcination at 550 °C (1 h in flowing N_2, followed by 6 h in O_2), to give the porous AMS-8 silicate.

(20) Kleitz, F.; Liu, D.; Anilkumar, G. M.; Park, I.-S.; Solovyov, L. A.; Shmakov, A. N.; Ryoo, R. *J. Phys. Chem. B* **2003**, *107*, 14296.

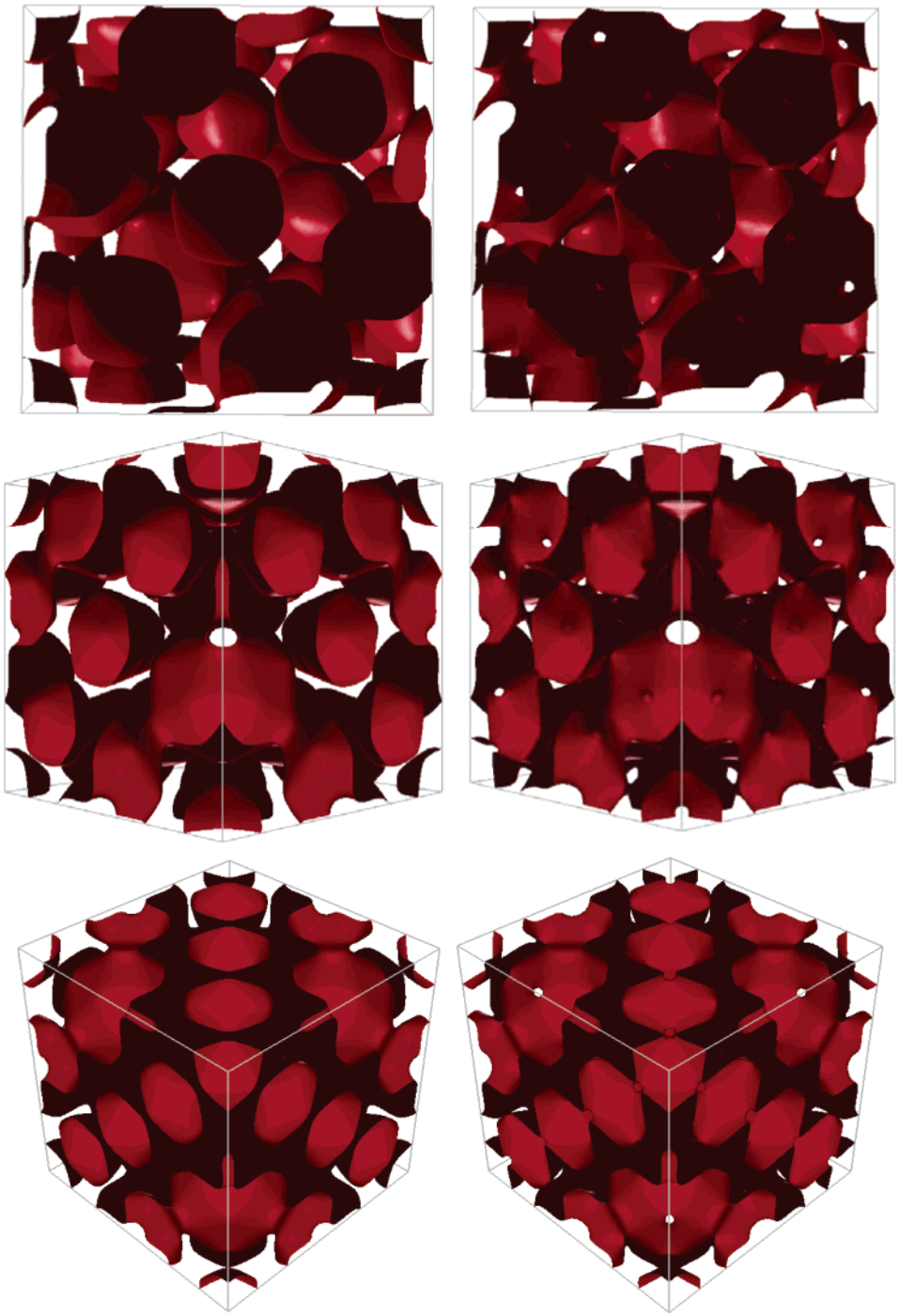

Figure 5. Electron density 3D reconstruction of the unit cell of AMS-8 viewed in perspective along the [100] (top), [110] (middle), and [111] (bottom) directions for threshold values 189 (left) and 199 (right). Only the outline of the cages is shown where light red corresponds to the interior surface of the cage. For threshold 189, large cages are connected via cavity windows to four additional large cages in a zigzag arrangement. This connecting window can be clearly seen as a pore opening parallel to the [110] orientation. Smaller cages are not connected. For threshold 199, large cages are connected to 12 individual smaller cages through small openings and to 4 additional larger cages through larger openings. Smaller cages are connected to each other through a single small pore opening.

XRD patterns were recorded on an MX Labo powder diffractometer equipped with Cu Kα radiation (40 kV, 20 mA) at the rate of 1.0°/min over the range of 1.5−10.0°.

The N_2 adsorption−desorption isotherms were measured at −196 °C on an ASAP202 Micromeritics Instrument. AMS-8 calcined mesoporous material was outgassed for a period of 6 h at 200 °C and 0.3 kPa pressure. The BET specific surface area was evaluated from the adsorption data in the relative pressure range from 0.05 to 0.3.[21] The total pore volume was estimated from the amount adsorbed at the relative pressure of 0.90. Pore size distribution curves were derived using NLDFT and for the sake of completeness the Horvath−Kawazoe (HK) method as developed by Saito and Foley.[22]

Transmission electron microscopy (TEM) was carried out with a JEOL-3010 microscope, operating at 300 kV (Cs 0.6 mm, resolution 1.7 Å). Images were recorded using a CCD camera (model Keen View, SIS analysis, size 1024 × 1024, pixel size 23.5 × 23.5 μm) at 30000−100000× magnification

(21) Gregg, S. J.; Sing, K. S. W. *Adsorption, Surface Area, and Porosity*; Academic Press: London, 1982.

(22) Saito, A.; Foley, H. C. *Microporous Mater.* **1995**, *3*, 531.

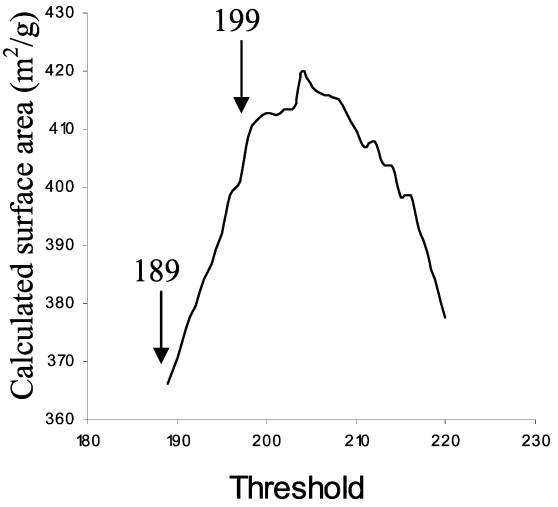

Figure 6. Plot of estimated surface area versus potential density threshold for AMS-8 mesocaged material. Estimates were derived computationally (see text for details).

using low-dose conditions. A typical HRTEM image observed from AMS-8 and its corresponding Fourier transform (FT) diffractogram are shown in Figure 3a. FT diffractograms, 3D-FT reconstructions, and electron potential density maps were generated using the SEMPER and MATHEMATICA software. Briefly, FT diffractograms are recorded along thin areas of HRTEM images from which extinction rules and hence the space group can be determined. Amplitudes and phases of FT diffraction peaks can be obtained. Phases were carefully extracted from several images, and amplitudes were determined from the highest quality image for each incidence [100], [011], [111], and [211] for the case of AMS-8. The space-group symmetry is then imposed on the derived amplitudes. Common reflections for different incidences are used to scale the amplitudes and derive the origin position. From the structure factors derived through combination of different data sets and after correction for the effect of contrast transfer function (CTF) assuming weak phases object approximation,[15] a 3D-electrostatic potential density map of the unit cell is obtained from the inverse FT of the structure factors. A software program written using C++ generated unit cell potential density maps shown in Figure 5.

Results and Discussion

The XRD pattern of calcined mesoporous material AMS-8 is shown in Figure 1. This shows low-angle peaks in the range $2\theta = 1.5-5°$, which can be indexed on the basis of a cubic structure with a unit cell parameter of $a = 183.4$ Å. The (111) reflection is expected at $2\theta = 0.83°$ for $Fd\bar{3}m$, which is below the range of our XRD powder diffractometer.

Figure 2 shows the nitrogen adsorption−desorption isotherm of calcined AMS-8. The porosity characteristics as derived through various data reduction methods are listed in Table 1. This isotherm is not atypical for mesoporous materials, and it is similar to those observed for cage-type mesoporous structures such as SBA-1, SBA-2, and FDU-1.[17,20] The surface area calculated using the BET method is 408.2 ± 1.83 m^2/g. The total pore volume by AMS-8 is 0.364 cm^3/g calculated from the amount adsorbed at a relative pressure 0.90. The isotherm curve is characterized by a broad, small, capillary condensation step in the adsorption branch occurring at $P/P_0 = 0.4$ and a hysteresis loop in the desorption branch of the isotherm. This has been previously associated with mesopore filling of cages.[19,21] Pore size distribution curves as calculated using the Horvath−Kawazoe (HK),[21] and the recently developed NLDFT method**,** give peak maxima centered on 6.2, 40.0, and 56.4 Å (HK) and 13.6, 37.0, and 55.0 Å (NLDFT). The latter allows accurate distinction between the volume of regular cavities and intrawall porosity. For AMS-8 these values are equal to 0.28 and 0.07 cm^3/g, respectively. The validity of the HK model for accurate pore size analysis of mesoporous solids is the subject of discussion and these results are shown for comparison purposes only. The NLDFT model on its own fails to estimate the extent of connectivities between cages. However, both methods identify that a bimodal system of mesocages is present.

Figure 3 shows HRTEM images of calcined AMS-8 material along the [100], [110], [111], and [211] directions. All images show a high degree of order. FT diffractograms shown as insets were calculated from thin areas of the images shown. Indexed reflections are consistent with a cubic unit cell with $a = 177.9$ Å. The FT diffractogram recorded along the [110] shows reflection conditions expected for $Fd\bar{3}m$ symmetry, namely, the presence of a *d*-glide plane, as indicated by the absence of the $h00$ reflections where $l = 4n + 2$. Table 2 shows normalized structure factors obtained from the FT reconstruction of calcined AMS-8 after CTF correction by assuming the origin to be centro-symmetric. Observable reflections are summarized as $\{hkl\colon\ h + k,\ h + l,\ k + l$ even$\}$, $\{0kl\colon\ k + l = 4n,\ k,\ l$ even$\}$, $\{hhl\colon\ h + l$ even$\}$, and $\{00l\colon\ l = 4n$ even$\}$, which are consistent with the $Fd\bar{3}m$ symmetry, and confirm unambiguously the space group.

To set a threshold value in the potential density to differentiate between the amorphous walls and the enclosed cavities, a plot of the relation between percentage volume fraction versus electron density is shown in Figure 4a. The total pore volume as determined from the N_2 adsorption−desorption isotherm of calcined AMS-8 is 0.365 cm^3/g. Assuming a silica wall density of 2.2 g/cm^3, this value corresponds to a pore volume fraction of ca. 44% and a threshold value of 189 (in a scale of 256). Large cages, 75 Å, and smaller cages, 52 Å, characterize the unit cell, where only larger cages are connected tetrahedrally to each other via small cage openings of 14 Å. Large cages are stacked in a zigzag fashion perpendicular to the [100] direction. The threshold value at which all cages are connected is 199 or a pore volume fraction of ca. 50%. In this case, small cages (56 Å) are tetrahedrally connected to each other via cage openings of 5 Å and connected to larger cages (76 Å) via pore openings of similar size. In addition, larger cages are connected to each other via pore openings of 25 Å. It is interesting to note that the relationship between pore volume fraction and cage dimensions is not linear, but the connectivity of cages varies considerably with increased pore volume.

Figure 4b shows a two-dimensional (2D) slice of the 3D-electrostatic potential density map of the unit cell of AMS-8 computed from the inverse FT of the structure factors as shown in Table 2. The slice shown is taken at $z = 7$ perpendicular to the [100] direction. Contour lines represent different values equivalent to different pore volume fractions. Figures 4c and 4d show similar slices, corresponding to pore volume fractions of 44 and

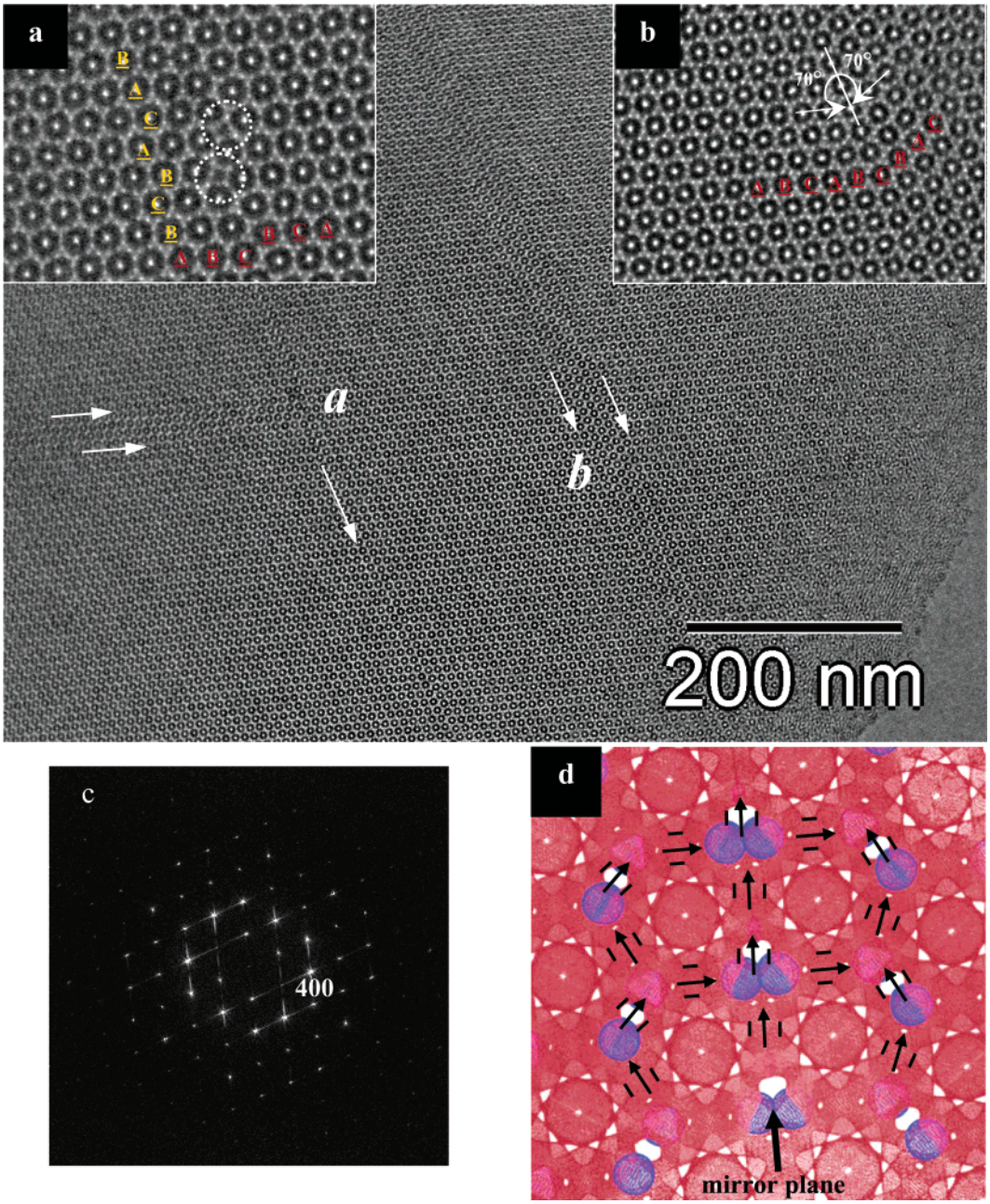

Figure 7. HRTEM image recorded on a thin particle of calcined AMS-8 with [110] incidence showing a large ordered region containing various stacking faults (highlighted by arrows). Insets shows images recorded at higher magnifications of regions a and b, where the presence of small structural features/cages can be discerned (highlighted in (a) by circles) as well as a mirror plane, (b). Figure 7c shows FT diffractogram generated from the image showing streaking. Figure 7d shows a schematic representation of the effect of stacking faults in (b) on the porous network of large cages (highlighted by blue spheres) in AMS-8. Arrows indicate the position of connectivities between large cages and white spots, corresponding to similar white contrast spots on the HRTEM image, showing the position of channels parallel to the [110] direction resulting from such connectivities.

50%, respectively (threshold values 189 and 199). The thickness of each slice corresponds to 1.834 Å. The center of large and small cages is located at Wyckoff positions 8b and 16c, respectively. Figure 5 shows reconstructed unit cells viewed along the [100], [110], and [111] orientations for pore volume fractions of 44 and 50%. The difference in connectivity between the two threshold values is easily appreciated. We believe the connectivity of cages in the AMS-8 structure to be between the two reconstructed models shown.

The low surface area measured for calcined mesocaged AMS-8, 408.2 m^2/g, in comparison to other cubic caged mesostructures such as SBA-1 (over 900 m^2/g) suggests that smaller cages are not fully accessible to the external surface. Surface area values based on the electron potential density maps generated from the 3D-FT reconstruction were approximated by subdividing the modeled unit cell into 100 slices along the *x*, *y*, and *z* directions. The surface area can be derived per pixel by calculating the area occupied by a plane cutting the subsliced pixels at a defined threshold value, where this plane approximation can be thought as the internal potential density surface of the modeled unit cell. By simple addition of all surface area values where this plane approximation can be applied, a value of the surface area can be estimated. The dependence of

surface area on threshold value is plotted in Figure 6. The estimated surface areas for threshold values 189 and 199 are 366.34 and 411.83 m^2/g, respectively. The BET calculated surface area is in close agreement with the estimated surface area at the higher threshold value, indicating that small and large cages in calcined AMS-8 are connected by small cage-openings of <14 Å.

One must be careful when comparing porosity data derived from the adsorption experiment and from HR-TEM images. Both methods have associated sources of error such as their dependence on the value taken for the density of silica in mesoporous materials, assumed to be that of amorphous silica (2.2 g/cm^3). We note here that although NLDFT allows distinction of the adsorption process in cavities of different sizes, it is only when a geometrical model is assumed that relevant information can be correlated to connectivity between cages. The 3D-FT reconstruction based on electron crystallography and HRTEM images does not preassume a geometrical model.

Structural defects have been observed by HRTEM previously for mesoporous materials and tend to be a feature of cage-type structures synthesized under basic conditions.[16,23] Figure 7 shows HRTEM images of calcined AMS-8 recorded along the [110] orientation. It is difficult to quantify the amount of defects in the whole structure. The arrangement of large cages parallel to the [110] direction forms a cylindrical channel arising from the connectivities between cavities, which have been measured to be between 14 and 25 Å. This cylindrical channel is viewed in the HRTEM image as white contrast spots. Insets (a) and (b) show stacking faults with a twinning-type relation (angle = 70°) perpendicular to the [110] orientation. These are identified as streaks in the FT diffractogram (Figure 7c). In defect-free regions of the mesostructure large cages are arranged, forming a zigzag porous network perpendicular to the [110] orientation. Along the mirror plane cages are arranged parallel to each other, their connecting pores/windows forming a straight channel perpendicular to the [110] direction. This is shown diagrammatically in Figure 7d. Furthermore, inset (a) shows features that arise as a result (highlighted by circles in the image) or cause the twinning in AMS-8. This may be indicative of a structural transformation in the AMS-8 structure.

The observation of stacking faults in AMS-8 associated with cubic and hexagonal packing of spherical micelles suggests the existence of a hexagonal end member that may form when the stacking faults are more frequent. Similarities can also be drawn from zeolites with similar symmetry. The face-centered cubic faujasite zeolite structure (FAU), for example, is well-known to form stacking fault disorders that lead to the formation of the hexagonal EMT structure.[23]

These results agree with the published literature on $Fd\bar{3}m$ surfactant phases in that they indicate the presence of a two-micelle system. However, discrepancies arise when we consider that previous reports suggest the $Fd\bar{3}m$ symmetry is only attainable by reverse micelles systems. We have no good explanation for this. However, the formation of ordered mesostructures critically depends on the interfacial interactions between the surfactants and the inorganic species. Clearly the presence of a co-structure directing agent has an increased effect on this interaction and may be the cause of the two-micelle system. We propose that prior to the addition of TEOS, only a certain number of micelles interact with the CSDA, forming what later become larger cages. The smaller size micelles arise from a failure of the CSDA to impart an increase in size due to either no condensation of the silane group surrounding the micelle or only partial condensation. This suggests the synthesis of AMS-8 is particularly susceptible to the condensation time of the CSDA prior to addition of TEOS as well as the amount of CSDA. Further investigations are being conducted.

Conclusions

The first result that can be unambiguously deduced from the present work is the determination of the space group of the mesoporous structure AMS-8. Reflection conditions are consistent with an $Fd\bar{3}m$ symmetry. The derived structure factors based on this space group show electrostatic potential density maps of AMS-8 composed of a bimodal arrangement of cages. There are 16 small (56.0 Å) and 8 large (76.0 Å) cages in the unit cell interconnected via cage windows of 14−25 Å (for large−large connectivities) and smaller windows of <5 Å (for large−small and small−small connections). Nitrogen adsorption data agree with our findings inasmuch as a bimodal pore size distribution is obtained when Horvath−Kawazoe and DFT models are used to analyze the isotherm. The surface area obtained experimentally using the BET method agrees with values calculated from the reconstructed structure by electron crystallography. These values are lower in comparison to other caged structures and suggest that accessibility to smaller cages in AMS-8 may be restricted as a result of the small connectivity. Values for surface area can be approximated from geometric and computational considerations of the re-constructed unit cell and add weight to our model of "partially" connected cages. Furthermore, the dependence of cage connections/windows can be studied in terms of total mesopore volume and surface area, allowing for further synthetic design. For example, it would be desirable to increase the size of cage windows/connections between large and small cages to facilitate diffusion of reactants and products for applications such as catalysis or gas separation. The synthesis of more open structures of AMS-8 is envisaged.

Finally, we highlight the importance of adsorption isotherm data coupled with electron crystallography as a method for the complete structural solution of mesoporous structures. Such methods when applied together offer accurate and reliable data that can be further used for the design and application of these complex and beautiful structures.

Acknowledgment. The authors thank Prof. T. Ohsuna and Dr. Y Sakamoto (Arrhenius Laboratory, Stockholm University) for many helpful discussions. Peter Oleynikov is thanked for preparing unit cell visualizations shown in Figure 5 from FT-reconstruction

(23) Zhou, W.; Hunter, H. M. A.; Wright, P. A.; Ge, Q.; Thomas, J. M. *J. Phys. Chem. B* **1998**, *102*, 6934. Hunter, H. M. A.; Garcia-Bennett, A. E.; Shannon, I. J.; Zhou, W.; Wright, P. A. *J. Mater. Chem.* **2002**, *12* (1), 20.

(24) Anderson, M.; Pachis, K. S.; Prebin, F.; Carr, S. W.; Terasaki, O.; Ohsuna, T.; Alfredsson, V. *Chem. Commun.* **1992**, *218*, 61.

data. We are grateful to AminoScience Lab, Ajinomoto Co., Inc., for providing *N*-acyl-amino acid and their salt surfactants. A.E.G.B. is grateful to the European Research and Training Network "Nanocage Materials" Grant No. HPRN-CT-2002-00193 for funding. This work was partly supported by the Swedish Science Council (VR), Core Research for Evolutional Science and Technology (CREST) of JST and BNRI, Japan (O.T.).

CM049398E